Quantitative Evaluation of Muscular Risks during Manual Load Handling using Vision-based System and Biomechanical Modeling*

Cosimo Patruno†1, Annaclaudia Bono[1,2], Tiziana D'Orazio[1], Grazia Cicirelli[1]

***Abstract*— Musculoskeletal disorders (MSDs) continue to represent one of the primary causes of pain, disability, and productivity loss, especially in work environments characterized by repetitive activities and manual material handling. This paper presents a vision-based system to investigate the muscular activities and risks associated with workers performing tasks such as lifting, carrying, and placing a load from a ground pallet to a shelf. A stereocamera setting, utilizing two commercial devices, is used to collect paired images of the actions performed by users. A deep learning model is employed to detect 2D skeletal keypoints, which are then projected into the 3D space using calibration data. Then, the obtained 3D keypoints of the worker's skeleton enable to derive the biomechanical model of the user by using the OpenSim framework. In this way, it is possible to import the movements of subjects and to perform the force and joint reaction analyses. Different performing metrics are introduced to quantify the duration of muscular activity, the biomechanical efficiency, and the physiological risk associated with different lifting modalities. The results confirm that the proposed approach can provide a first indication of workplace operational configurations that minimize physiological effort and muscular risk for workers.**

Keywords — Muscular analysis, multi-camera system, Ergonomics, workplace environments, human well-being

I. INTRODUCTION

Musculoskeletal disorders (MSDs) are among the most common work-related health problems and represent a major cause of pain, disability, and productivity loss worldwide. This issue is particularly relevant in industrial and logistics environments characterized by repetitive actions [1]–[3] and manual material handling, such as lifting, carrying, and placing loads. According to occupational health studies, improper lifting strategies and poor workplace design significantly increase biomechanical load and the risk of musculoskeletal injury [4], [5].

Conventional ergonomic risk assessment methods, including standardized indices such as the NIOSH lifting equation, OWAS, RULA, and REBA, are widely adopted in industrial practice due to their simplicity and low implementation cost [6]–[8]. These approaches provide a fast, intuitive evaluation of biomechanical risk. However, they are primarily observational and rely heavily on expert judgment. As a consequence, they offer limited accuracy in capturing dynamic movements, subject-specific anthropometric characteristics, and internal biomechanical quantities such as muscle forces and joint reaction loads [9].

To overcome these limitations, motion analysis systems based on optical tracking and biomechanical modeling have been proposed. Marker-based motion capture combined with musculoskeletal simulation platforms, such as OpenSim, enables accurate estimation of joint kinematics, muscle activations, and internal forces [10], [11]. Despite their high accuracy, these systems require expensive equipment, complex setup procedures, and controlled laboratory environments, which strongly limit their applicability in real industrial scenarios.

Recent advances in computer vision and deep learning have enabled markerless human pose estimation methods that extract skeletal keypoints directly from RGB images [12]–[14]. Approaches such as OpenPose and AlphaPose have demonstrated high accuracy in 2D pose estimation across a wide range of conditions [15], [16]. By leveraging multi-view or stereo camera configurations, 2D keypoints can be reconstructed in 3D space, enabling non-invasive motion analysis at a significantly reduced cost [17]. However, most existing vision-based studies focus primarily on kinematic analysis or posture recognition, without explicitly linking the reconstructed motion to biomechanical and physiological indicators relevant for MSD risk assessment.

In this paper, we propose a comprehensive framework that integrates a low-cost stereo vision system, deep learning–based 2D keypoint extraction, and biomechanical modeling using the OpenSim framework to analyze muscular activity and physiological risk during manual material-handling tasks. This framework explicitly bridges the markerless vision-based motion systems with the musculoskeletal force estimation associated to the motion. The translation of 3D motion data into a biomechanical domain enables the extraction of physiological indicators that are not accessible through 3D kinematics alone.

The main contributions of this work are: (i) a non-invasive and low-cost acquisition setup based on commercial devices; (ii) the integration of vision-based 3D skeletal reconstruction with subject-specific biomechanical modeling to estimate muscle forces and joint reactions; (iii) the definition of performance metrics to quantify muscular activation duration, biomechanical efficiency, and physiological risk associated with different lifting strategies. The obtained results provide an initial indication of workplace configurations that can reduce muscular effort and mitigate the risk of MSDs.

II. METHOD

This section explains the 3D skeleton extraction, the biomechanical model computation, and the muscular analysis for quantitatively evaluating the muscular risks during the manual handling of loads by workers. In this way, both correct and incorrect postures during task execution can be readily identified.

A. 3D skeleton extraction

To perform the muscular evaluation, the 3D skeleton of a single subject performing the tasks is extracted. Starting from the original 2D video frames, a multi-person pose estimation approach based on advanced computer vision and deep learning techniques is employed to automatically detect and track human body poses.

*We acknowledge financial support under the National Recovery and Resilience Plan (NRRP), Mission 4, Component 2, Investment 1.1, Call for tender No. 104 published on 02-02-2022 by the Italian Ministry of University and Research (MUR), funded by the European Union – NextGenerationEU– Project Title "INnovative Tools for the Enhancement of manufacturing systems for smart and Resilient Operators (INTERO)" – CUP 2022FCLRXT - Grant Assignment Decree No. 1401 adopted on 18-09-2024 by the Italian Ministry of University and Research (MUR).

[1] Institute of Intelligent Industrial Technologies and Systems for Advanced Manufacturing (STIIMA) of the National Research Council (CNR), Bari, Italy.

[2] Polytechnic University of Bari, Bari, Italy

†Corresponding author: cosimo.patruno@cnr.it

In particular, we adopted the Halpe26 model integrated within the AlphaPose framework, as introduced in [16]. This model is able of estimating 26 anatomical keypoints — also referred to as 2D joints — providing a detailed and reliable representation of the human posture, as shown in Figure 1.

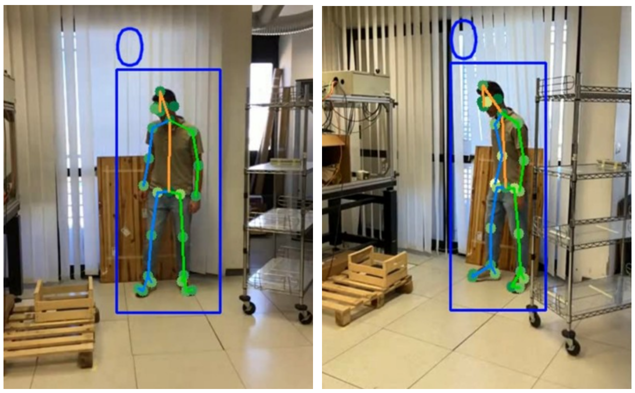

Fig. 1. Multi-view perspective of the user while performing one task. The 2D skeleton is superimposed on the images.

To ensure accurate and reliable 3D reconstructions, a dedicated calibration procedure was performed. This step is essential for estimating both the intrinsic camera parameters — such as focal length and lens distortion — and the extrinsic parameters, which define the relative position and orientation of the cameras within the multi-view setup. For this purpose, a 4×5 checkerboard pattern with a square size of 35 mm was employed, as shown in Figure 2.

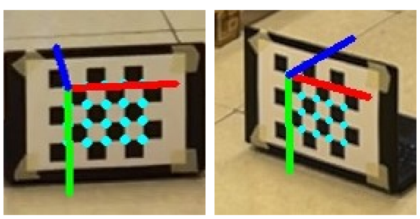

Fig. 2. Camera view perspectives of the checkerboard pattern from the two devices.

In a calibrated acquisition setup, the 3D position of each 2D keypoint detected in the images can be accurately reconstructed, thereby enabling the computation of the biomechanical model associated with the user under observation. The accuracy of the reconstructed 3D skeleton using our procedure was assessed using the mean reprojection error, which was on average $10.6\, px$ (about $34.6\ mm$) across all joints. The impact of these inaccuracies on biomechanical outputs is mitigated by temporal filtering and by aggregating individual muscles into functional macro-groups, which reduces the sensitivity of the proposed indices to local pose estimation noise, as discussed in the experimental section.

B. Biomechanical model computation

The computed 3D keypoints of the skeleton are then used to derive the biomechanical model of the user by using OpenSim [18], an open-source and extensible software platform for modeling, simulating, and analyzing the neuromusculoskeletal system. The full-body musculoskeletal model (*.osim*) proposed by Rajagopal [19], incorporating the Beaucage-Gauvreau adaptation [20], has been used. The model includes muscles and articular joints for actuating the lower and upper body (see Fig. 3).

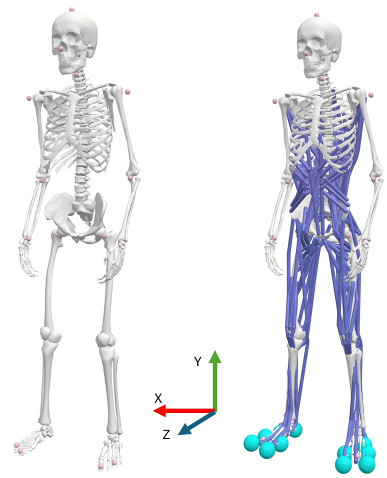

Fig. 3. OpenSim body model with the 3D markers (pink dots) and the muscles (blue cylinders in the left image). The cyan spheres represent the contact probes for GRF computation.

By constructing the trace file (*.trc*), which contains the trajectories of 3D keypoints over time, it becomes possible to incorporate the movements into OpenSim by mapping the 3D keypoints to the model's 3D markers. This allows the model to be scaled using the subject's biometrics, after which the executed motion can be accurately computed for dynamic simulations. Using the Inverse Kinematics (IK) module of OpenSim, joint angles can be estimated, producing a motion (*.mot*) file that is essential for force and joint reaction analyses. Indeed, the kinematic data contained in the *.mot* file represent the time histories of joint angles for all body segments in the model.

Since force plates were not available for this study, ground reaction forces (GRFs) were estimated to obtain a more accurate assessment of forces and joint reactions. To this end, the second version of OpenGRF [21], a free OpenSim tool based on the MATLAB API, was utilized. Starting from the subject-specific musculoskeletal model (*.osim*) and the kinematics file (*.mot*), OpenGRF computes both the GRFs and the center of pressure (CoP). As shown in Figure 3, the cyan contact probes located at the model's feet are used to estimate ground forces during motion. These ground contact forces are derived from estimates of foot–ground interactions and applied as external constraints during the optimization procedure. Subsequently, for each analyzed frame, the muscle forces that satisfy the body's dynamic equilibrium are computed. From these forces, quantitative indicators of muscle activity can then be extracted.

C. Quantitative metrics for muscular and joint activity

To reduce the complexity of the musculoskeletal model and facilitate a functional interpretation of the results, the muscles and articular joints are organized into five macro-groups, defined based on their location and mechanical contribution. This subdivision enables the concise representation of the main kinematic chains involved, while maintaining a direct link between the computed force quantities and the biomechanical actions that generate them. The five macro-groups are defined as follows:

- *Shoulder/Arm Muscles*: Includes the articular joints responsible for shoulder flexion, adduction, and rotation, as well as the elbow flexors and the muscles involved in forearm pronation–supination. These elements control load positioning and upper-limb stabilization during the grasp and placement phases.
- *Trunk Muscles*: Includes the principal spinal erectors and spinal muscles responsible for trunk flexion, extension, and rotation. They ensure trunk stability and postural control

throughout the movement, assuming a predominant role in incorrect executions characterized by marked lumbar flexion.
- *Hip Muscles*: Represents the group of muscles acting on the hip joint, including the extensors, flexors, adductors, and deep rotators of the hip. Among these are the three portions of the gluteus maximus, the gluteus medius and minimus, the iliopsoas, the tensor fasciae latae, the sartorius, and the main adductors. These muscles constitute the primary generator of push during the rising phase, transmitting force from the pelvis to the lower limbs.
- *Upper Leg Muscles*: Includes the thigh muscles acting on the knee joint, responsible for extension and flexion movements. These comprise the quadriceps femoris (rectus femoris, vastus medialis, lateralis, and intermedius) and the hamstrings (biceps femoris, semimembranosus, semitendinosus). This group governs body configuration during the bending phase and generates vertical thrust when lifting the load.
- *Lower Leg Muscles*: Includes the leg and ankle muscles responsible for foot control and interaction with the ground. These include the triceps surae (medial and lateral gastrocnemius and soleus), the dorsiflexors (tibialis anterior, extensor digitorum longus, extensor hallucis longus), the deep flexors (tibialis posterior, flexor digitorum longus, flexor hallucis longus), and the peroneal (fibular) muscles. They ensure plantar stability and regulate the distribution of vertical load and ground reaction forces.

This classification, summarized in Table I for completeness, allows analysis of muscle activations in terms of functional chains rather than individual anatomical units, facilitating the biomechanical interpretation of the results.

TABLE I. Classification of the muscles into the five macro-groups considered, distinguished by right (_r) and left (_l) sides.

Macro-group	Muscle and articular joint denomination
Shoulder/Arm Muscles	shoulder_flex_r, shoulder_flex_l, shoulder_add_r, shoulder_add_l, shoulder_rot_r, shoulder_rot_l, elbow_flex_r, elbow_flex_l, pro_sup_r, pro_sup_l
Trunk Muscles	lumbar_ext, lumbar_bend, lumbar_rot
Hip Muscles	glmax1_r, glmax1_l, glmax2_r, glmax2_l, glmax3_r, glmax3_l, glmed1_r, glmed1_l, glmed2_r, glmed2_l, glmed3_r, glmed3_l, glmin1_r, glmin1_l, glmin2_r, glmin2_l, glmin3_r, glmin3_l, iliacus_r, iliacus_l, psoas_r, psoas_l, piri_r, piri_l
Upper Leg Muscles	grac_r, grac_l, tfl_r, tfl_l, recfem_r, recfem_l, sart_r, sart_l, addbrev_r, addbrev_l, addlong_r, addlong_l, addmagDist_r, addmagDist_l, addmagIsch_r, addmagIsch_l, addmagMid_r, addmagMid_l, addmagProx_r, addmagProx_l, vasint_r, vasint_l, vaslat_r, vaslat_l, vasmed_r, vasmed_l, recfem_r, recfem_l, bflh_r, bflh_l, bfsh_r, bfsh_l, semimem_r, semimem_l, semiten_r, semiten_l
Lower Leg Muscles	soleus_r, soleus_l, gaslat_r, gaslat_l, gasmed_r, gasmed_l, tibant_r, tibant_l, edl_r, edl_l, ehl_r, ehl_l, tibpost_r, tibpost_l, fhl_r, fhl_l, fdl_r, fdl_l, perbrev_r, perbrev_l, perlong_r, perlong_l

The force signals of individual muscles and articular joints are first filtered using a moving-average filter over short time windows to reduce residual numerical discontinuities without altering the signal dynamics. Subsequently, the muscles are aggregated into the defined macro-groups. For bilateral regions, such as the lower and upper limbs, the average is computed between the right and left sides. For the trunk, the aggregation is performed over the entire set.

To quantify the relative duration of muscular activity, the $Duty_{x\%}$ index is used, defined as the percentage of time during which the force developed by a muscle group exceeds the $x\%$ of its own maximum value. Mathematically, for each group i, the index is expressed as:

$$\mathrm{Duty}_{x\%} = \frac{\sum_{t=1}^{T} \left(F(t) > \frac{x}{100} \cdot F_{\max} \right)}{T} \times 100 \tag{1}$$

where T is the total number of frames of the movement and x represents the percentage threshold. The $Duty_{x\%}$ therefore measures the time fraction during which a muscle district operates under significant load conditions, providing a direct indication of the cumulative physiological stress sustained during execution of the task. In this study, $x = 50$ has been set.

To concisely quantify the biomechanical efficiency and the physiological risk associated with different lifting modalities, two indicators are introduced, derived from the mean $\mathtt{Duty}_{50\%}$ values calculated over the five muscle macro-groups: the Distribution of Load Index (DOI) and the Muscular Risk Index (MRI). The DOI represents the ability of the muscular system to distribute the load along the lower kinetic chain and is defined as:

$$DOI = \frac{D_{\text{Hip}} + D_{\text{Upper Leg}} + D_{\text{Lower Leg}}}{D_{\text{Shoulder/Arm}} + D_{\text{Trunk}}} \tag{2}$$

where D_{Hip}, $D_{\text{Upper Leg}}$, $D_{\text{Lower Leg}}$, D_{Trunk}, and $D_{\text{Shoulder/Arm}}$ represent the $\mathtt{Duty}_{50\%}$ values computed for the main body clusters. A high DOI value indicates that load distribution is distributed predominantly to the lower districts, a biomechanically efficient condition associated with lower ergonomic risk. Conversely, a low DOI indicates excessive involvement of the trunk and upper limb muscles, suggesting improper load transfer and an increased risk of lumbar and scapular overload. In fact, from a physiological perspective, a prolonged activation of trunk and shoulder muscles under high relative load is commonly associated with increased lumbar compression and scapulohumeral stress, which are well-recognized risk factors for work-related MSDs.

To make the results easier to read, the Muscular Risk Index (MRI) is also defined as the normalized inverse of the DOI:

$$MRI = \text{round}\left(\frac{1}{DOI} \times 100 \right) \tag{3}$$

In this way, higher MRI values correspond to less favorable muscular configurations, characterized by a greater concentration of effort in the upper body, whereas lower values indicate correct and physiologically efficient load distribution.

III. RESULTS

This section describes the experimental framework underlying the analysis presented in Section II, which investigates the muscular risk during the lifting, carrying, and repositioning of a wooden crate weighing 3 kg from a pallet to a metallic shelf, as shown in Figure 1. The experiments involved six participants with heights ranging from 165 cm to 193 cm. Each participant performed a sequence of movements. The load is picked up from a pallet placed on the ground and positioned on shelves at four different heights (30 cm, 80 cm, 130 cm, and 180 cm), representative of common working conditions in industrial and logistics environments. For each participant, eight acquisitions were recorded: four classified as “correct”, characterized by controlled bending with knee flexion, a neutral trunk, and moderately flexed arms during the lifting phase, thus involving a low muscular risk; and four “incorrect”, in which the movement was mainly performed through trunk flexion, with fully extended arms and limited involvement of the lower limbs, resulting in less ergonomic postures and greater loading of the lumbar region (please refer to Figure 4) that might involve increasing of muscular risks.

Fig. 4. Sketch of correct (low muscular risk) and incorrect postures (high muscular risk).

Two iOS-based tablets have been used to collect the videos of users. The analysis aims to quantify the muscular risk associated with the lifting and load-positioning task under different execution techniques and shelf heights. The entire analysis process has been developed in the MATLAB environment and structured as an automated pipeline that automatically extracts quantitative indicators of muscle activity. This procedure enabled a detailed evaluation of muscular risk throughout the entire motion cycle, from bending and grasping to lifting and repositioning. Specifically, by exploiting the 3D positions of the hands obtained from the 3D skeleton computation, the movement of the user can be segmented into five phases: (1) start, (2) bending, (3) grasping the load, (4) lifting the load, and (5) placing the load on the shelf. This segmentation enables further analyses focused on specific time intervals of interest.

The temporal analysis of muscle forces enables the observation of how the contributions of different body regions evolve during motion. Figures 5 and 6 show, respectively, the force trends for the five muscle macro-groups in a trial classified as correct and incorrect movement for the same subject. Each chart reports the force over time, divided into the five phases of the task (start, bending, grasping, lifting, and placement) together with the $\mathtt{Duty}_{50\%}$ threshold, which indicates the value corresponding to 50% of the maximum force recorded for the considered group.

In the correct movement (Figure 5), a pattern is observed that is consistent with the biomechanics expected for ergonomic lifting. During the bending phase, the *Hip Muscles* and *Upper Leg Muscles* show a marked increase in force, indicating coordinated activation of the gluteal muscles and the knee extensors during controlled flexion. In the subsequent grasping phase, the load remains distributed over the lower limbs, with a limited but steady contribution from the *Lower Leg Muscles*, which stabilize the plantar posture. During the ascent (lifting), the hip and thigh groups reach their peak force, while the contribution of the *Trunk Muscles* remains moderate, indicating a stable trunk posture without excessive lumbar flexion. Finally, in the placement phase, the force of the upper groups (*Shoulder–Arm Muscles*) increases slightly to allow precise positioning of the load, but overall remains below overload thresholds. The overall profile is regular and well distributed, with the lower-limb muscles supporting most of the load and the trunk serving as a stabilizing element. This configuration highlights an efficient movement strategy consistent with the correct execution of the lift.

In the incorrect movement (Figure 6), the forces developed by the *Hip Muscles* and *Upper Leg Muscles* are reduced, indicating limited involvement of the lower limbs in generating push. By contrast, a clear increase is seen in the *Trunk Muscles* and *Shoulder–Arm Muscles*, especially during the bending and placement phases. This suggests that the lift is performed mainly through trunk flexion and arm pulling, with greater involvement of the lumbar and scapular musculature. During the raising phase, the force of the lower groups remains relatively low, while activation peaks in the upper regions exceed the $\mathtt{Duty}_{50\%}$ threshold multiple times, indicating a prolonged and repeated load in biomechanically less favorable regions. This behavior is indicative of an inefficient compensatory strategy, in which the lack of controlled knee flexion and gluteal activation is offset by increased spinal extensor forces and excessive use of the upper limbs.

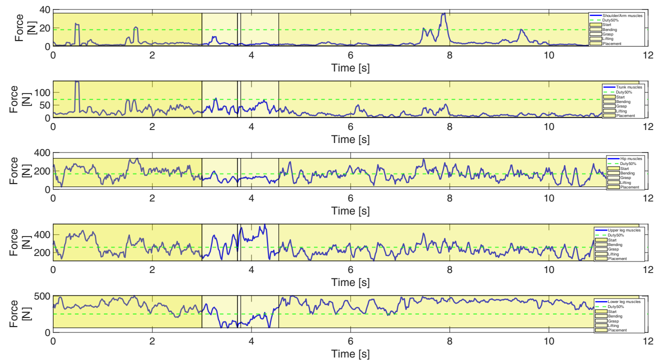

Fig. 5. Temporal trend of muscle forces for the functional macro-groups (relating to acquisition #4 of the correct movement of subject #1).

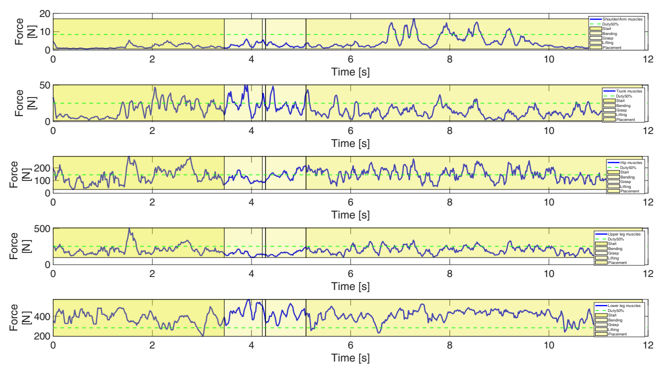

Fig. 6. Temporal trend of muscle forces for the functional macro-groups (relating to acquisition #4 of the incorrect movement of subject #1).

The comparison between the two conditions clearly highlights the difference in the distribution of internal load: in the correct trial the work is done mainly by the lower regions, whereas in the incorrect trial the push is transferred to the upper segments, with a consequent increase in the risk of lumbar and scapular overload. This observation constitutes quantitative evidence of the link between execution technique and muscular strategy, showing how proper coordination of the lower kinetic chain makes it possible to reduce the stress on the upper regions.

A direct indication of the cumulative physiological stress sustained by muscles and articular joints during the execution of the task can be obtained by observing the $\mathtt{Duty}_{50\%}$ values of macro-groups. Specifically, Figure 7 summarizes the mean $\mathtt{Duty}_{50\%}$ values for the five muscular macro-groups, comparing trials performed with correct and incorrect technique.

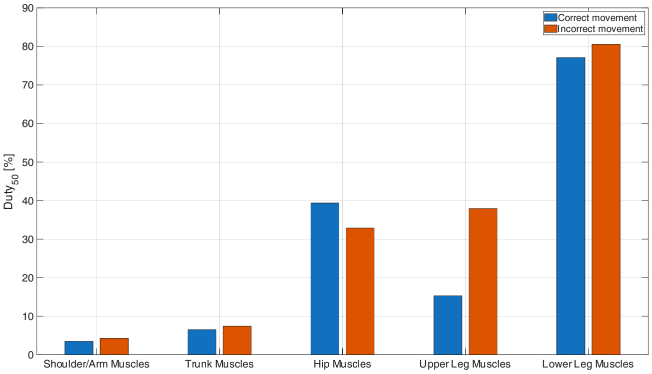

Fig. 7. Mean $\mathtt{Duty}_{50\%}$ values of the five muscular macro-groups for all correct and incorrect executions.

A clear difference in the distribution of activity is observed between upper and lower districts. In correct executions, the *Hip Muscles* and *Upper Leg Muscles* show higher $\mathtt{Duty}_{50\%}$ values, indicating prolonged involvement of the hip and knee extensor musculature, consistent with lifting performed through controlled leg flexion. Conversely, the values for the *Shoulder–Arm Muscles* and *Trunk Muscles* are lower, thus indicating that the thrust is generated mainly by the lower limbs and not by the trunk or the arms. This behavior represents a biomechanically appropriate distribution of load, with a predominance of work in districts less subject to joint overload. In the incorrect movement, the load distribution is altered with respect to the biomechanically optimal condition. The *Trunk Muscles* and *Shoulder–Arm Muscles* show slightly higher $\mathtt{Duty}_{50\%}$ values than in the correct case, indicating greater involvement of the spine and upper limbs in load control. This increase does not imply that these districts become the primary force generators — the role remains with the lower-limb musculature — but it highlights an abnormal and unnecessary contribution of the trunk and shoulders, symptomatic of an inefficient compensatory strategy. At the same time, an increase in $\mathtt{Duty}_{50\%}$ is also observed for the *Lower Leg Muscles*, indicating that the calves intervene more intensely in maintaining balance and plantar stabilization due to limited knee flexion and a greater forward shift of the body.

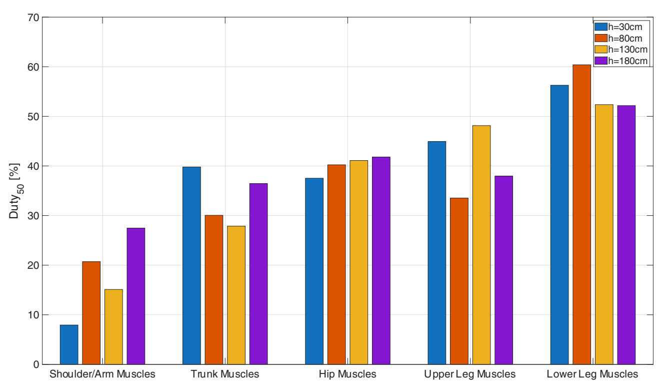

Fig. 8. Trend of mean $\mathtt{Duty}_{50\%}$ as a function of shelf height.

Figure 8 shows the analysis of the mean $\mathtt{Duty}_{50\%}$ across all acquisitions (correct and incorrect) as a function of the placement shelf heights (30, 80, 130, and 180 cm). From inspection of the charts, a direct correlation emerges between shelf height and distribution of effort:

- the *Shoulder/Arm Muscles* are more highly stressed at the shelf height of 180 cm, where the arm must operate in prolonged flexion above shoulder level, with a consequent increase in the scapulohumeral torque;
- the *Trunk Muscles* show an increase in $\mathtt{Duty}_{50\%}$ at both very low and very high heights, indicating that both configurations impose marked postural deviations, while intermediate heights appear to be the most favorable for spinal alignment and load distribution;
- the *Hip Muscles* are less stressed at the lowest shelves (30 cm), which represent the most favorable biomechanical conditions, since the lift occurs with a more balanced participation of the lower kinetic chain and less stress on the hip extensor musculature;
- for the quadriceps (*Upper Leg Muscles*), the intermediate height H2 (80 cm) is the most efficient, whereas the calves (*Lower Leg Muscles*) show a higher $\mathtt{Duty}_{50\%}$ at the low and intermediate shelves (30–80 cm), where they contribute significantly to stabilizing the body and maintaining balance during the bending and ascent phases; at greater heights (180 cm) their activity decreases because the primary task is carried out by the upper body parts.

The overall comparison among the four configurations shows that the intermediate heights (H2–H3) represent the ergonomically optimal conditions, as they ensure the most balanced distribution of load among the muscle macro-groups. The extreme heights (H1 and H4) instead entail an increase in the activity of the upper or lower districts, leading to a deterioration in overall mechanical efficiency. The overall sum of the mean $\mathtt{Duty}_{50\%}$ values confirms this trend, with the following order of efficiency: H3 (184.6%) $\approx$ H2 (184.9%) $<$ H1 (186.5%) $<$ H4 (195.8%), where lower values correspond to a more homogeneous distribution and therefore a lower risk of overload.

The MRI (Muscular Risk Index) values were computed for the six subjects, considering all eight acquisitions per subject. The distribution of MRI by considering the correct and the incorrect movement strategy is shown in Figure 9.

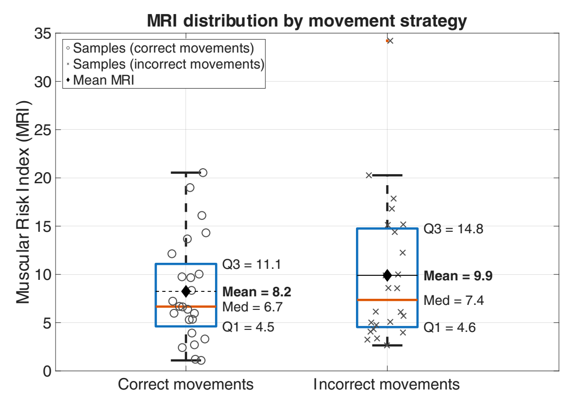

Fig. 9. Muscle Risk Index (MRI) distribution for the considered acquisitions.

The MRI index summarizes the overall level of muscular effort required to perform each task, providing an integrated measure of the risk of functional overload. By comparing the two distributions, the lower quartile (Q1) is comparable between the two conditions ($Q1 = 4.5$ for correct and $Q1 = 4.6$ for incorrect movements), indicating that low muscular load conditions may occur in both strategies. The incorrect executions exhibit a higher median ($Med = 7.4$) and upper quartile ($Q3 = 14.8$) in comparison with the correct case. Moreover, an increased interquartile range ($IQR = Q3 - Q1 = 10.2$) and a mean ($Mean = 9.9$) shifted toward higher values are observable for the incorrect case compared to the correct one ($IQR = 6.5$ and $Mean = 6.7$). This indicates that high muscular risk events occur more frequently in incorrect postures, thereby involving less robust biomechanical loading conditions and potentially greater hazard. Overall, the distribution of scores indicates that correct movements tend to have lower average values, whereas incorrect movements show higher scores, in agreement with greater stress on the trunk and upper limb muscle groups. The most extreme case is represented by the maximum value of $MRI = 33$, related to subject 5 during acquisition 8, which corresponds to an incorrect movement performed on the highest shelf (180 cm). This value, clearly higher than all the others, may indicate a very demanding biomechanical condition due to the combination of a long lever arm and a high working height. This subject is indeed the shortest in the sample set (165 cm), and this characteristic amplifies the mechanical effects of the lever arm, significantly increasing the flexion moment on the trunk and shoulder.

Despite some overlaps between the two distributions, the mean MRI value for correct executions is 6.7, whereas for incorrect ones it is 9.9, with a difference $\Delta = 2.2$. This confirms that correct movements, on average, produce a lower muscular load, more evenly distributed along the lower kinematic chain of the body, whereas incorrect movements concentrate the effort on the trunk and upper limbs, resulting in lower biomechanical efficiency and higher muscular stress or activation. In fact, from a physiological perspective, a prolonged activation of trunk and shoulder muscles under high relative load is commonly associated with increased lumbar compression and scapulohumeral stress, which are well-recognized risk factors for work-related MSDs.

IV. CONCLUSIONS

This paper presented a preliminary study aimed at analyzing muscular activity and biomechanical risk in manual material handling tasks by combining computer vision, deep learning, and biomechanical modeling. The proposed pipeline integrates a stereocamera setup with a deep learning–based 2D pose estimation framework and 3D reconstruction to derive subject-specific musculoskeletal models within the OpenSim environment. This approach enables the quantitative assessment of muscle activations, joint reaction forces, and physiological effort associated with different lifting modalities. The results demonstrate that the proposed methodology is capable of providing meaningful indicators of muscular load and biomechanical efficiency, highlighting how specific task configurations and execution strategies can reduce physical strain and potential injury risk. Although the study is preliminary and limited to controlled experimental conditions, the outcomes confirm the feasibility of the approach as a support tool for ergonomic evaluation and workplace design. Future work will focus on validating the methodology on a larger number of subjects, extending the analysis to more complex and realistic industrial scenarios, and integrating additional sensing modalities to further improve accuracy and robustness. Other future developments will investigate the integration of machine learning techniques for automatic classification of execution quality and real-time risk prediction based on the extracted biomechanical indicators.

ACKNOWLEDGMENT

The authors are deeply thankful to Michele Attolico and Paola Romano for their technical and administrative support.

REFERENCES

[1] C. Patruno, G. Cicirelli, L. Romeo, and T. D'Orazio, "Analysis of input data configurations in cnn-based human action recognition for assembly task," in *2025 11th International Conference on Control, Decision and Information Technologies (CoDIT)*, vol. 1, 2025, pp. 22–27.

[2] C. Patruno, L. Romeo, A. Bono, T. D'Orazio, and G. Cicirelli, "Skeleton-based human action recognition for manufacturing in assembly task by deep learning," in *Multimodal Sensing and Artificial Intelligence for Sustainable Future*, vol. 13570, International Society for Optics and Photonics. SPIE, 2025, p. 135701D.

[3] M. V. A. Gallón, C. Patruno, G. Mata, C. Domínguez, and G. Cicirelli, "Transformer-based human action recognition for fine-grained industrial assembly tasks," in *IECON 2025 – 51st Annual Conference of the IEEE Industrial Electronics Society*, 2025, pp. 1–6.

[4] C. Greggi, V. V. Visconti, M. Albanese, B. Gasperini, A. Chiavoghilefu, C. Prezioso, B. Persechino, S. Iavicoli, E. Gasbarra, R. Iundusi, and U. Tarantino, "Work-related musculoskeletal disorders: A systematic review and meta-analysis," *Journal of Clinical Medicine*, vol. 13, no. 13, 2024.

[5] R. Govaerts, B. Tassignon, J. Ghillebert, B. Serrien, S. De Bock, T. Ampe, I. El Makrini, B. Vanderborght, R. Meeusen, and K. De Pauw, "Prevalence and incidence of work-related musculoskeletal disorders in secondary industries of 21st century europe: a systematic review and meta-analysis," *BMC musculoskeletal disorders*, vol. 22, no. 1, p. 751, 2021.

[6] D. Kee, "Systematic comparison of owas, rula, and reba based on a literature review," *International Journal of Environmental Research and Public Health*, vol. 19, no. 1, p. 595, 2022.

[7] M. Gómez-Galán, Á.-J. Callejón-Ferre, J. Pérez-Alonso, M. Díaz-Pérez, and J.-A. Carrillo-Castrillo, "Musculoskeletal risks: Rula bibliometric review," *International journal of environmental research and public health*, vol. 17, no. 12, p. 4354, 2020.

[8] M. A. Wahyudi, W. A. Dania, and R. L. Silalahi, "Work posture analysis of manual material handling using owas method," *Agriculture and Agricultural Science Procedia*, vol. 3, pp. 195–199, 2015.

[9] S. J. Thomas, J. A. Zeni, and D. A. Winter, *Winter's biomechanics and motor control of human movement*. John Wiley & Sons, 2022.

[10] R. Zaman, Y. Xiang, R. Rakshit, and J. Yang, "Hybrid predictive model for lifting by integrating skeletal motion prediction with an opensim musculoskeletal model," *IEEE Transactions on Biomedical Engineering*, vol. 69, no. 3, pp. 1111–1122, 2021.

[11] A. Seth, M. Sherman, J. A. Reinbolt, and S. L. Delp, "Opensim: a musculoskeletal modeling and simulation framework for in silico investigations and exchange," *Procedia Iutam*, vol. 2, pp. 212–232, 2011.

[12] L. Romeo, C. Patruno, G. Cicirelli, and T. D'Orazio, "Multi-view skeleton analysis for human action segmentation tasks," in *International Conference on Pattern Recognition Applications and Methods*, 2025, pp. 579–586.

[13] C. Patruno, V. Renò, G. Cicirelli, and T. D'Orazio, "Multimodal people re-identification using 3d skeleton, depth, and color information," *IEEE Access*, vol. 12, pp. 174 689–174 704, 2024.

[14] L. Romeo, C. Patruno, G. Cicirelli, and T. D'Orazio, "Deep learning methods with iterative-boosting for performing human action recognition in manufacturing scenarios," in *2025 11th International Conference on Control, Decision and Information Technologies (CoDIT)*, vol. 1, 2025, pp. 835–840.

[15] Z. Cao, G. Hidalgo, T. Simon, S.-E. Wei, and Y. Sheikh, "Openpose: Realtime multi-person 2d pose estimation using part affinity fields," *IEEE transactions on pattern analysis and machine intelligence*, vol. 43, no. 1, pp. 172–186, 2019.

[16] H.-S. Fang, J. Li, H. Tang, C. Xu, H. Zhu, Y. Xiu, Y.-L. Li, and C. Lu, "Alphapose: Whole-body regional multi-person pose estimation and tracking in real-time," *IEEE Transactions on Pattern Analysis and Machine Intelligence*, 2022.

[17] D. Pavllo, C. Feichtenhofer, D. Grangier, and M. Auli, "3d human pose estimation in video with temporal convolutions and semi-supervised training," in *Proceedings of the IEEE/CVF conference on computer vision and pattern recognition*, 2019, pp. 7753–7762.

[18] A. Seth, J. L. Hicks, T. K. Uchida, A. Habib, C. L. Dembia, J. J. Dunne, C. F. Ong, M. S. DeMers, A. Rajagopal, M. Millard, *et al.*, "Opensim: Simulating musculoskeletal dynamics and neuromuscular control to study human and animal movement," *PLoS computational biology*, vol. 14, no. 7, p. e1006223, 2018.

[19] A. Rajagopal, C. L. Dembia, M. S. DeMers, D. D. Delp, J. L. Hicks, and S. L. Delp, "Full-body musculoskeletal model for muscle-driven simulation of human gait," *IEEE transactions on biomedical engineering*, vol. 63, no. 10, pp. 2068–2079, 2016.

[20] E. Beaucage-Gauvreau, W. S. Robertson, S. C. Brandon, R. Fraser, B. J. Freeman, R. B. Graham, D. Thewlis, and C. F. Jones, "Validation of an opensim full-body model with detailed lumbar spine for estimating lower lumbar spine loads during symmetric and asymmetric lifting tasks," *Computer methods in biomechanics and biomedical engineering*, vol. 22, no. 5, pp. 451–464, 2019.

[21] A. Di Pietro, F. Di Puccio, and L. Modenese, "Opengrf: Predicting ground reaction forces and moments during daily living activities in opensim," 2025.